Bifunctional photocatalysts display proximity-enhanced catalytic activity in metallaphotoredox C–O coupling

Luigi Dolcini,[a] Andrea Solida,[a] Daniele Lavelli,[a] Andrés Mauricio Hidalgo-Núñez,[a] Tommaso Gandini,[a] Matthieu Fornara,[a] Alessandro Colella,[a] Alberto Bossi,[b] Marta Penconi,*[b] Daniele Fiorito,[c] Cesare Gennari,[a] Alberto Dal Corso,[a] Luca Pignataro*[a]

[a] L. Dolcini, A. Solida, D. Lavelli, A. M. Hidalgo-Núñez, Dr. T. Gandini, M. Fornara, A. Colella, Prof. C. Gennari, Dr. A. Dal Corso, Prof. L. Pignataro
Dipartimento di Chimica
Università degli Studi di Milano
Via C. Golgi, 19 – 20133 Milano (Italy)
E-mail: luca.pignataro@unimi.it, marta.penconi@cnr.it

[b] Dr. A. Bossi, Dr. M. Penconi
Istituto di Scienze e Tecnologie Chimiche "Giulio Natta" (SCITEC) del Consiglio Nazionale delle Ricerche (CNR), via Fantoli 16/15, 20138 Milano, Italy
SmartMatLab Center, via C. Golgi 19, 20133 Milano (Italy)

[c] Dr. D. Fiorito
Dipartimento di Chimica, Materiali e Ingegneria Chimica "Giulio Natta", Politecnico di Milano, P.za Leonardo da Vinci 32, 20133 Milano (Italy)

Supporting information for this article is given via a link at the end of the document.

Abstract: Dual catalytic reactions may be made more effective through an improved integration of the catalytic cycles achieved using bifunctional catalysts. Herein we describe new bifunctional photocatalysts consisting of a photoactive donor-acceptor cyanoarene unit linked to a bipyridine ligand moiety that can bind transition metals. The bifunctional photocatalysts were synthesized in 3-5 steps form commercially available compounds and fully characterized in terms of photophysical properties, which are strongly affected by the type of linkage used (C vs. O) to connect the cyanoarene core to the ligand. Catalytic tests carried out in the Ni-catalyzed C-O cross-coupling of alcohols to aryl bromides promoted by visible light have shown that the bifunctional systems are more active than the corresponding 'dual catalytic systems' (i.e., not covalently bound), taking advantage of the proximity between the two catalytic moieties (Ni-complex and photocatalyst). The best bifunctional dyes were tested with several alcohols and aryl halides, giving good yields at low catalytic loading (0.5-2 mol%).

Introduction

The bifunctional approach to catalysis has been exploited in many instances to achieve improved yield, selectivity or even novel types of reactivity. Owing to proximity, two (or more) covalently linked functional groups may operate synergistically and combine different types of activation more effectively than the corresponding 'dual systems' (i.e., employing two distinct catalysts). This concept is best represented in organocatalysis, some archetypical catalysts (e.g., proline) being bifunctional, as well as many others developed by rational design.[1] Moreover, several bifunctional transition metal catalysts have been reported: beside the ligand necessary to bind the metal, these systems possess an additional functional group capable of substrate binding/activation and (or) formation of "supramolecular bidentate ligands".[2] In the context of blossoming interest for visible light

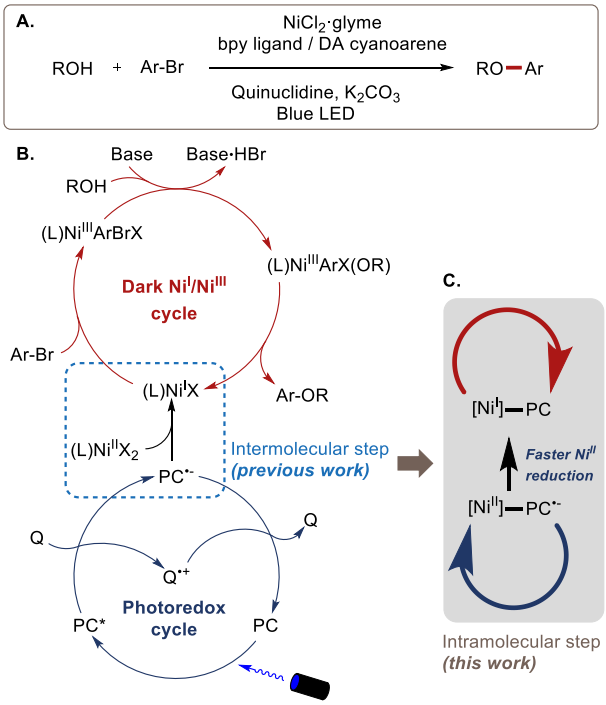

Scheme 1. DA cyanoarene-promoted metallaphotoredox catalytic C-O coupling (A), its mechanism (B), and the foreseen advantage of using a bifunctional dye (C). PC = photocatalyst; Q = quinuclidine.

photocatalysis observed in the last two decades, several bifunctional photocatalysts have been reported.[3] Indeed, many visible light-promoted transformations are actually dual catalytic reactions,[4] and thus hold an evident potential for a bifunctional approach. So far, most efforts have been devoted to enantioselective catalysts, and photocatalysts have been linked to several types of chiral catalysts such as amines,[5] lactams,[6] thioureas,[7] Brønsted acids,[8] Cinchona-derived ammonium

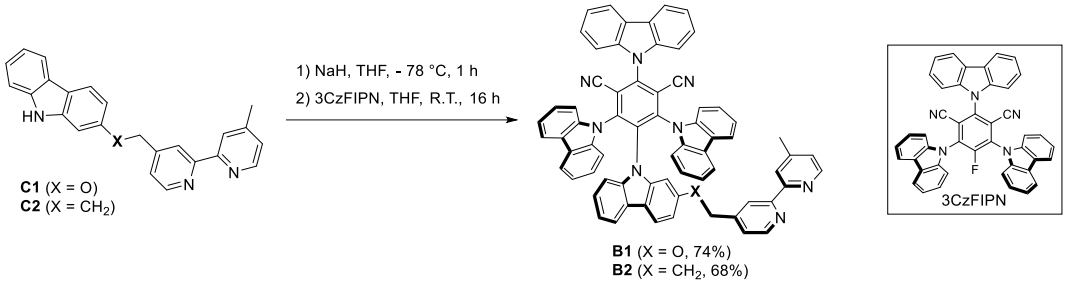

Scheme 2. Synthesis of the bifunctional photocatalysts **B1** and **B2**.

salts[9] and Ni-BOX complexes.[10] Although transition metal photocatalysts have been also employed,[5b,6b,c] most bifunctional photocatalysts rely on organic dyes, with thioxanthone taking the lion's share. We envisioned that the bifunctional approach, besides the enantioselectivity issue, could generally enhance the performance of dual catalytic reactions by ensuring a better integration between the relevant catalytic cycles.

Building on our expertise in metallaphotoredox catalytic C-O and C-N cross-couplings,[11] we set to investigate this issue with new catalysts featuring an organic photocatalyst connected to a 2,2'-bipyridine ligand. We selected the Ni-photoredox cross-coupling between alcohols and aryl bromides (Scheme 1 A)[11,12] as test bench to assess our bifunctional approach because the $Ni^{II} \rightarrow Ni^{I}$ reduction step of the catalytic cycle (Scheme 1 B),[11,13] operated by $PC^{\bullet -}$, was expected to benefit from proximity between metal and photocatalyst (Scheme 1 C).[14] This paper describes the synthesis of two such bifunctional photocatalysts and the study of their catalytic properties in Ni-photoredox C-O cross-coupling reactions.

Results and Discussion

Synthesis of the bifunctional dyes

Owing to their high catalytic activity, ready accessibility and easy purification, donor-acceptor (DA) cyanoarenes have been successfully proposed as catalysts in photoredox organic reactions.[11,15,16] Thus, we chose these compounds as optimal candidates for incorporation into bifunctional systems.[17] As shown by Bergens and co-workers,[18] the different S_NAr reactivity of the *ortho*/*para* vs. *meta* positions of perfluorocyanoarenes offers the opportunity to sequentially introduce *different carbazole (Cz) residues* onto the central cyanoarene core. We thus placed the functionalized carbazole moiety **C1** (synthesized from 2-hydroxycarbazole as described in the Supporting Information) onto the 3CzFIPN core[11,18] by S_NAr reaction with the corresponding sodium salt, obtaining the bifunctional dye **B1** in good yield (Scheme 2). This dye can be seen as a DA-cyanoarene-conjugate possessing a bidentate ligand for binding a catalytic metal.

Since we expected that the introduction of an oxygen substituent in one carbazole could remarkably affect the electronic and photocatalytic properties, we also prepared the bifunctional photocatalyst **B2**, possessing a CH_2 instead of an O linkage, by the same S_NAr protocol (Scheme 2). The functionalized carbazole substrate **C2** was synthesized as shown in the Supporting Information. Moreover, two **B1**-analogs featuring different linkers were also prepared, but found less active than **B1** (see the Supporting Information), thus confirming the crucial importance of size and geometry of the linker to attain an effective cooperation between the catalytic sites.

Assessment of proximity effect

To evaluate the effect of proximity, the catalytic properties of bifunctional dye **B1** (Scheme 3 B) were compared with those of a dual catalytic system composed by the same, non-linked parts in 1:1 ratio, i.e. 4,4'-dimethyl-2,2'-dipyridyl (4,4'-dmbpy) and DA-cyanoarene **R1** (Figure 1, prepared as described in the Supporting Information), bearing a benzyloxy substituent at the same position as **B1**. In the benchmark reaction of *n*-hexanol and 4-bromoacetophenone, the *in situ*-formed Ni-complexes of both catalytic systems gave good yields at relatively high catalytic loading (2 mol%). However, to our delight, when the loading was reduced to 1 mol% and 0.5 mol%, the bifunctional system proved clearly superior to the dual, which suffered from an evident yield drop (Scheme 3 A vs. B).

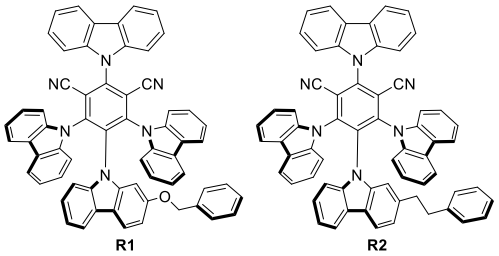

Figure 1. The reference dyes employed in this study.

The higher activity of the bifunctional system [1:1 **B1** / $NiCl_2$(glyme)] compared to the corresponding dual catalytic system [1:1:1 **R1** / $NiCl_2$(glyme) / 4,4'-dmbpy] was confirmed by kinetic studies on the same reaction (Figure 2). The kinetic profiles of the reaction promoted by the bifunctional and by the dual catalyst were strikingly different: the former reached full conversion within 50 min with a downward concave profile both at 1 mol% (Figure 2 A) and at 0.5 mol% catalyst loading (Figure 2 B). The latter showed a nearly linear kinetic profile which, at 0.5 mol% catalyst loading (Figure 2 B), did not reach full conversion even after 24 hours.

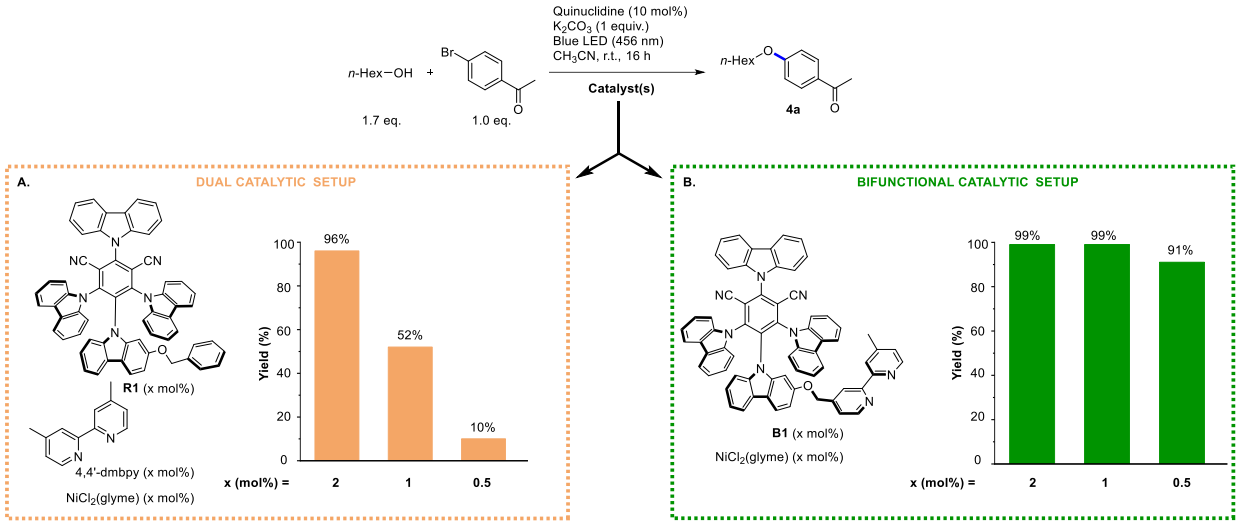

Scheme 3. Comparison between the bifunctional ligand **B1** and the corresponding dual catalytic system at different catalytic loadings. Yields were determined by ^{1}H NMR using 1,3,5-trimethoxybenzene as internal standard.

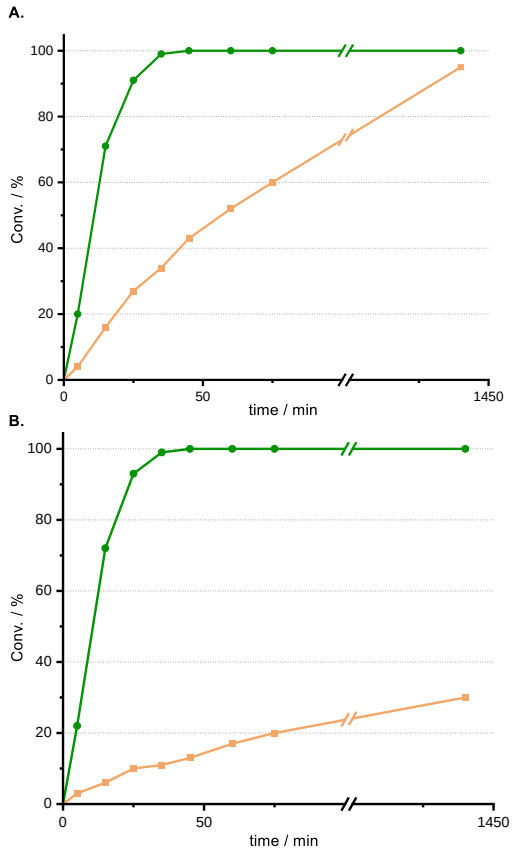

Figure 2. Kinetic profile of the reaction between *n*-hexanol and 4-bromoacetophenone with the bifunctional setup [1:1 **B1** / $NiCl_2$(glyme)] (-●-) and the dual catalytic setup [1:1:1 **R1** / $NiCl_2$(glyme) / 4,4'-dmbpy] (-■-) at 1 mol% (A) and at 0.5 mol% (B) catalyst loading. Conversions were determined by ^{1}H NMR.

The bifunctional dye **B2** was tested in the benchmark C-O coupling reaction and compared with the corresponding dual catalytic setup involving the reference dye **R2** and 4,4'-dmbpy. We found that also with **B2** a proximity effect is operating. At 0.5 mol% loading, the bifunctional setup showed a slightly steeper kinetic profile than the dual catalytic setup, which still gave full conversion (see the Supporting Information). The difference between the two systems became more evident below 0.5 mol% catalyst loading, under which conditions the bifunctional system afforded higher yields than the dual one (Scheme 4 B vs. A). Thus, bifunctionality brings higher catalytic activity for both the O-linked dye **B1** and the CH_2-linked dye **B2**, but this is more evident in the former case. Indeed, the O-linked dye can take greater

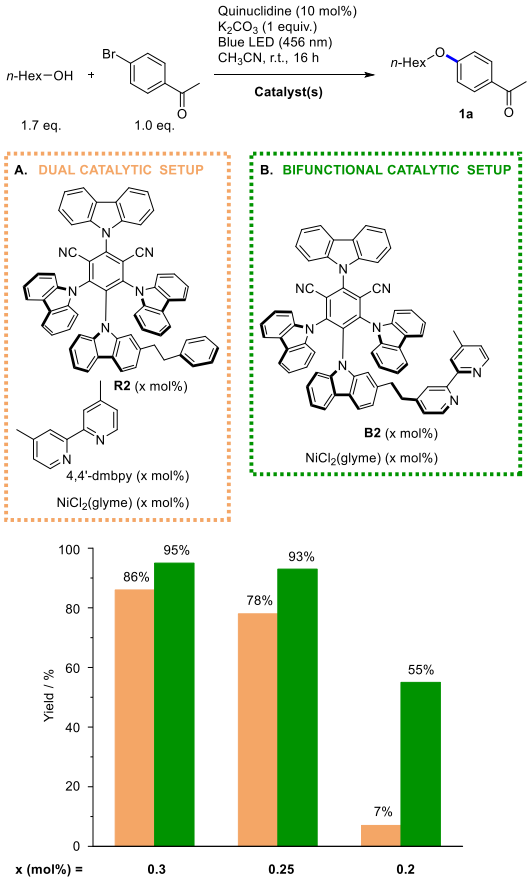

Scheme 4. Comparison between the bifunctional ligand **B2** and the corresponding dual catalytic system at different catalytic loadings. Yields were determined by ^{1}H NMR using 1,3,5-trimethoxybenzene as internal standard.

advantage from proximity because its photoactive core is intrinsically less performing due to fast non-radiative de-excitation (see below).

As a matter of fact, the bifunctional systems **B1** and **B2** allowed to obtain similar yields in the C-O coupling of several aryl bromides with *n*-hexanol and other primary and secondary alcohols (Scheme 5), with **B1** giving slightly better results in most instances (except when poorly nucleophilic 2,2,2-trifluoroethanol was tested). Notably, the yield of the **B2**-promoted synthesis of ether **1a** was not affected by a 10× scale-up (i.e., 5 mmol instead of 0.5 mmol scale) using the same light source of the standard experiments (one Kessil light).

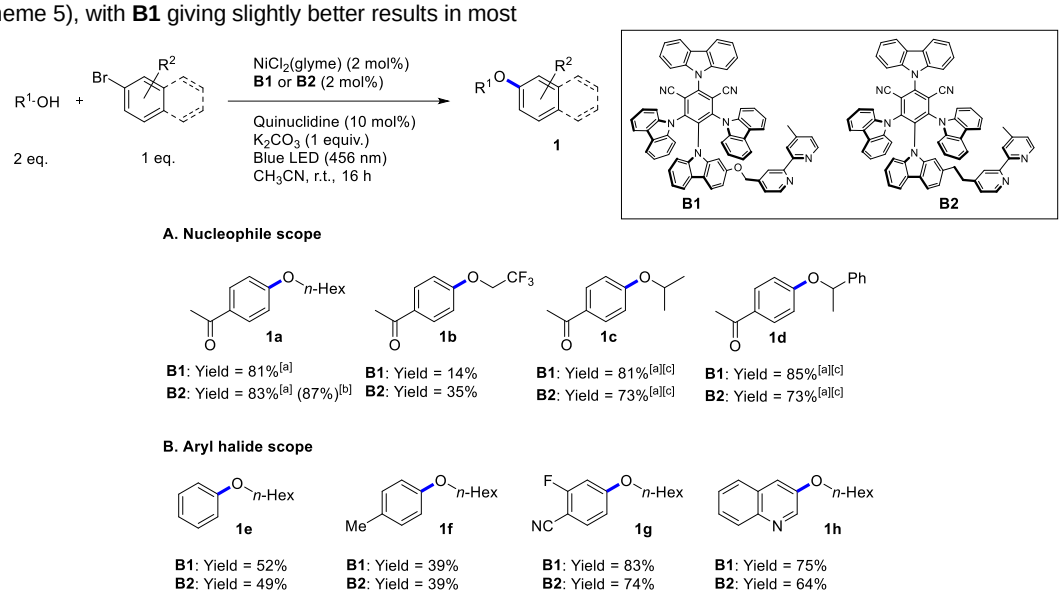

Scheme 5. Substrate scope investigation in C-O coupling in the presence of the bifunctional dyes **B1** and **B2**. Reactions were carried out on a 0.5 mmol scale. Isolated yields are shown. [a] 0.5 mol% loading of Ni and bifunctional dye. [b] Reaction carried out on a 5 mmol scale (10× scale up). [c] 4 equiv. of alcohol used.

Photophysical studies

The photophysical properties of the photocatalysts were investigated by UV−vis absorption and steady-state and time-resolved photoluminescence spectroscopy. The UV−vis absorption spectra of **B1**, **B2**, **R1**, **R2** and 4CzIPN were recorded at 298 K in diluted acetonitrile (Figure 3 A) and toluene solution (Figure S8 in the Supporting Information). The newly synthesized photocatalysts exhibit absorption spectra very similar to the parent compound 4CzIPN, characterized by strong absorption below 300 nm attributed to localized π-π* transitions of the aromatic and carbazole units. The bipyridine moiety in **B1** and **B2** determines the higher extinction coefficient at 285 nm with respect to the other compounds. At lower energy, all the molecules are characterized by identical broad absorption bands: a first one centered at 364 nm accounting for the n-π* transitions, and a second transition at 430 nm, ascribed to the charge transfer (CT) from the carbazolyl donor unit to the benzonitrile acceptor moiety. The steady-state photoluminescence spectra in diluted acetonitrile and toluene solutions at 298 K (Figure 3 B) showed a broad and structureless emission band. Moreover, the photocatalysts **B1** and **R1**, having an electron donor oxygen bound to the carbazole, display in both solvents an emission red-shifted of ca. 10 nm compared to the other systems. We observed a solvatochromic effect from toluene to the more polar acetonitrile as the maximum of the low-energy absorption band blue-shifts of about 10 nm and the emission peak red-shifts of about 55 nm. Together, the solvatochromic effect, the relevant Stokes Shift in polar acetonitrile and the absence of vibrational structure in the emission band, point to the charge transfer character of the excited state which is therefore stabilized in polar solvent.

Time-resolved experiments show a double-exponential decay character of the photoluminescence with a prompt fluorescence (PF) component in the order of nanoseconds and a delayed fluorescence (DF) component in the microsecond range for all the compounds (see Table 1, and Table S4-5 in the Supporting Information). The quantum yields (Φ) of PF and DF were calculated from measurements in the presence and in the absence of oxygen. The newly synthesized photocatalysts are highly emissive in toluene, and both Φ_{PF} and Φ_{DF} are comparable to those of 4CzIPN. In acetonitrile, a decrease of the quantum yields was observed for **B2**, **R2** and 4CzIPN, as already reported in polar solvents,[19] whereas the luminescence is suppressed in **B1** and **R1**, probably accounting for a fast non-radiative relaxation of the photoexcited species promoted by the presence of oxygen atom.[20] In summary, the oxygen-sensitive fluorescence and the double-exponential decay provide evidence of the nature of TADF (Thermally Activated Delayed Fluorescence) emitters of **B1**, **B2**, **R1**, **R2**, just as the well-known 4CzIPN.

The *in situ* formation of the **B1**-Ni complex was proved by high-resolution ESI-MS analysis of a 1:1 **B1**/[$NiCl_2$(glyme)] solution in acetonitrile that clearly showed the **B1**-$NiCl^+$ peak as the main signal (see the Supporting Information). A spectroscopic titration of a **B1** solution in DMF at the addition of $NiCl_2$(glyme) aliquotes, reveals the growth of a new absorption peak at 302 nm (see the Supporting Information). The absorbance did steadily grow until Ni^{II}/**B1** ratio of 1 was reached, but higher Ni^{II}/**B1** ratio did not produce further changes, thus confirming that a 1:1 complex had formed.

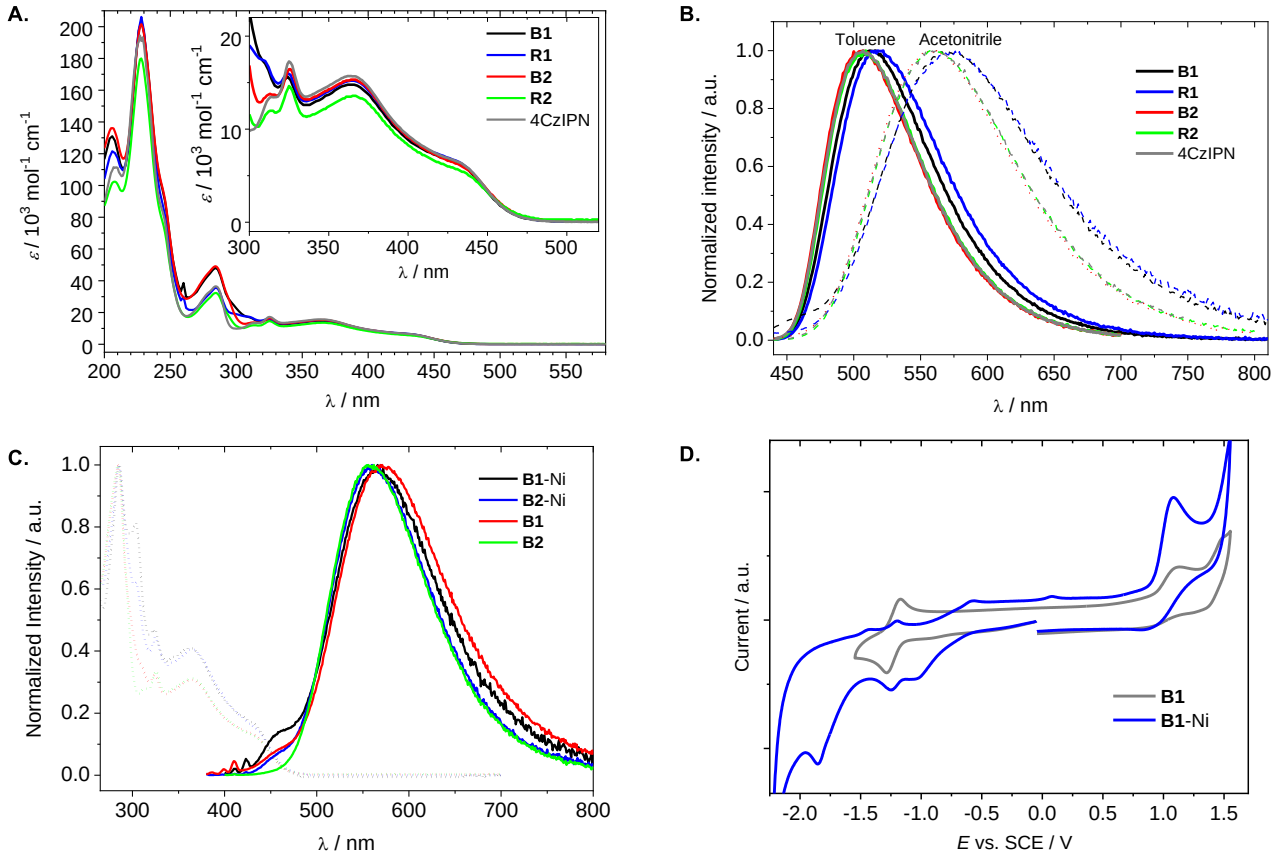

Figure 3. A. Absorption spectra of free photocatalysts in acetonitrile. B. Normalized emission spectra of free photocatalysts measured in toluene (solid line) and acetonitrile (dot line). C. Normalized absorption (dot line) and emission (solid line) spectra of **B1**, **B2**, **B1**-Ni and **B2**-Ni in acetonitrile. D Representative voltammograms for the **B1** and **B1**-Ni systems.

The photophysical properties of the Ni-complexes **B1**-Ni and **B2**-Ni are reported in Figure 3 C and Table 1. The absorption spectra are identical to their analogous free photocatalysts except for the appearance of a shoulder at 302 nm, ascribed to the complex absorption as already observed in the spectroscopic titration. The photoluminescence of the complexes is superimposable to those of **B1** and **B2**. The complexes display TADF character, nevertheless, the PF and DF quantum yields are negligible for **B1**-Ni, as for **B1**, and are reduced for **B2**-Ni with respect to **B2**. The excited state lifetimes are considerably reduced when the photocatalysts are bound to the metal.

The electrochemical properties of **B1** and **B2**, their Ni-complexes (**B1**-Ni and **B2**-Ni) and their reference dyes **R1** and **R2** were studied by cyclic voltammetry in acetonitrile solution. The full set of results is reported in the Supporting Information (Figure S12), whereas Figure 3 D contains two representative voltammograms (**B1** and **B1**-Ni). Complexes **B1**-Ni and **B2**-Ni were prepared *in situ* adding $NiCl_2$(glyme) to the solution of free photocatalysts. The redox potentials of **B1**, **B2**, their Ni-complexes **B1**-Ni and **B2**-Ni and the reference dyes **R1** and **R2** are shown in Table 1 and in the Supporting Information (Table S6).

Table 1. Photophysical and electrochemical properties of the photocatalysts involved in this study measured in acetonitrile under N_2.

#	Photocatalyst	$\lambda_{max,em}$ / nm	Φ_{PF}[a]	Φ_{DF}[b]	τ_{PF} / ns	τ_{DF} / µs	$E_{0,0}$ / eV	$E_{1/2}$ ($PC^*/PC^{\bullet-}$) / V[c,d]	E_{onset} ($PC^{\bullet+}/PC^*$) / V[c,d]	E_{onset} ($PC^{\bullet+}/PC$) / V[c]	$E_{1/2}$ ($PC/PC^{\bullet-}$) / V[c]
1	**B1**	571	0.01	< 0.01	30.1	1.16	2.68	1.46	-0.99	1.69	-1.22
2	**B1**-Ni[e]	565	0.02	< 0.01	3.7	0.12	2.68	1.46	-1.12	1.56	-1.22[f]
3	**R1**	572	0.01	< 0.01	18.0	1.71	2.64	1.42	-1.00	1.64	-1.22
4	**B2**	559	0.14	0.08	20.0	2.09	2.64	1.42	-1.11	1.53	-1.22
5	**B2**-Ni[e]	560	0.09	< 0.01	8.6	0.50	2.64	1.42	-1.10	1.54	-1.22[f]
6	**R2**	560	0.14	0.10	20.2	2.07	2.63	1.41	-1.09	1.54	-1.22
7	4CzIPN	560	0.15	0.08	18.2	1.64	2.67	1.44	-1.17	1.50	-1.23

[a] Measured under air. [b] Difference between Φ measured under N_2 and under air. [c] Electrochemical potentials are referenced to the saturated calomel electrode (SCE). [d] Excited state potentials were calculated according to the following formulas: E ($PC^*/PC^{\bullet-}$) = E ($PC/PC^{\bullet-}$) + $E_{0,0}$; E ($PC^{\bullet+}/PC^*$) = E ($PC^{\bullet+}/PC$) – $E_{0,0}$. [e] Complex generated *in situ*. [f] Potential associated to the reduction of the benzonitrile core; the reduction and oxidation potentials of Ni are omitted in this table (whole data reported in Supporting Information). The zero-zero vibrational state excitation energy $E_{0,0}$ was calculated from the intersection point between the absorption and emission spectra after the maximum intensity of emission is normalized to the absorbance at the excitation wavelength.

Overall, we found that all systems undergo a complex multielectronic oxidation at potentials over 1.99 V vs. SCE (onset around 1.4 V), similarly to the behavior already observed for 4CzIPN (see the Supporting Information). In contrast, a reversible monoelectronic reduction is observed, at $E_{1/2}$ = -1.22 V vs. SCE, for all the studied systems, and this potential is not affected by the substitution pattern on the carbazole moiety. This would imply a process mostly localized on the benzocyano core of the dye (see calculations in the Supporting Information, Table S7). A further, irreversible reduction is detected below -1.81 V vs. SCE. Notably **B1** and **B2**, featuring a bipyridine group, show a further reduction peak below -2.21 V vs. SCE attributed to the monoelectronic reduction of the bipyridine system (4,4'-dmbpy was measured as reference, see the Supporting Information). As expected, complexes **B1**-Ni and **B2**-Ni show a further reductive redox process at a potential slightly less negative compared to the reduction of the benzocyano core (-1.22 V vs. SCE), which is compatible with the reduction process associated to the $Ni^{II}|Ni^{I}$ couple (E = -1.11 V vs. SCE), and an oxidation around 1.09 V ascribed to the $Ni^{III}|Ni^{II}$ process (see the $NiCl_2$(dtbbpy) redox properties in Figure S12).[11,21]

Table 2. Quenching of the photocatalysts by quinuclidine under the reaction conditions.[a]

#	Dye	K_{SV} / mol^{-1} L	$\tau_{0,DF}$ / µs	k_q / mol^{-1} L s^{-1}
1	**B1**-Ni	623	0.116	$5.39 \cdot 10^9$
2	**R1**	5663	1.44	$3.93 \cdot 10^9$
3	**B2**-Ni	2260	0.431	$5.24 \cdot 10^9$
4	**R2**	9921	2.10	$4.72 \cdot 10^9$
5	4CzIPN	10625	1.67	$6.36 \cdot 10^9$

[a] Data collected from Stern-Volmer plots of delayed lifetimes (excitation at 375 nm) in Ar-degassed acetonitrile.

The Stern-Volmer quenching experiments (see the Supporting Information for the graphs) confirm that the photocatalysts employed in this study (**B1**-Ni, **B2**-Ni, **R1** and **R2**) are quenched by quinuclidine with comparable quenching constants (k_q in Table 2), despite the strong reduction of lifetimes observed in the Ni-complexes (**B1**-Ni, **B2**-Ni) with respect to the reference photocatalysts **R1** and **R2** (Table 2, entries 1, 3 vs. 2, 4). This is consistent with the C-O coupling mechanism that we previously proposed (Scheme 1).[11,13] Moreover, the improved performances of the bifunctional photocatalysts with respect to the dual systems at decreased loading suggest that an intramolecular step involving the $Ni^{II} \rightarrow Ni^{I}$ reduction could operate after the photocatalyst is quenched by quinuclidine.

Conclusion

In this paper we have described a bifunctional catalytic approach involving conjugation of an organic dye to a bpy ligand that can bind transition metals. Using the metallaphotoredox Ni-catalyzed C-O cross-coupling as model reaction, we have demonstrated that proximity between the two catalytic moieties (i.e., the metal complex and the dye) is beneficial for catalytic activity, which is higher than the one displayed by the corresponding dual catalytic system. The bifunctional photocatalysts have been shown able to promote the coupling of several primary and secondary alcohols to aryl bromides at low catalytic loading. This work represents one of the first examples of bifunctional DA-cyanoarene,[11,13] and – to the best of our knowledge – the first in which these TADF-emitters are linked to a bidentate ligand. We believe that the proof-of-concept provided by this work may serve as a basis to further implement the 'bifunctional approach' in photocatalysis, exploring other types of metal, reactivity and catalyst design.

Supporting Information

Supplementary Figures, experimental methods, and spectral data for all new products are within the Supporting Information. The authors have cited additional references within the Supporting Information.[22]

Acknowledgements

We thank the European Commission (European Union's Horizon Europe research and innovation programme, Marie Skłodowska-Curie Grant Agreement no. 101119574 "NextBase") for a Ph.D. fellowship (to A. M. H.-N.) and financial support. Mass spectrometry analyses were performed at the Mass Spectrometry facility of the Unitech COSPECT at the University of Milan (Italy). M.P. and A.B. gratefully acknowledge Regione Lombardia and Fondazione Cariplo for funding the SmartMatLab Centre project.

Keywords: metallaphotoredox catalysis • bifunctional catalysis • donor-acceptor cyanoarenes • cross-coupling • visible light

[1] a) X. Liu, L. Lin, X. Feng, *Chem. Commun.* **2009**, 6145-6158; b) O. V. Serdyuk, C. M. Heckel, S. B. Tsogoeva, *Org. Biomol. Chem.* **2013**, *11*, 7051-7071; c) P. Chauhan, S. Mahajan, U. Kaya, D. Hack, D. Enders, *Adv. Synth. Catal.* **2015**, *357*, 253-281; d) Z.-W. Zhang, S.-W. Liu, H.-P. Huang, Y.-H. Xie, R.-C. Huang, Y.-Q. Deng, N. Lin, *RSC Adv.* **2023**, *13*, 31047-31058.

[2] a) A. J. Sandee, J. N. H. Reek, *Dalton Trans.* **2006**, 3385-3391; b) S. Carboni, C. Gennari, L. Pignataro, U. Piarulli, *Dalton Trans.* **2011**, *40*, 4355-4373; c) R. H. Morris, *Acc. Chem. Res.* **2015**, *48*, 1494-1502; d) D. J. Dixon, *Beilstein J. Org. Chem.* **2016**, *12*, 1079-1080; e) L. Pignataro, C. Gennari, *Chem. Rec.* **2016**, *16*, 2544-2560; f) R. H. Morris, *Chem. Rec.* **2016**, *16*, 2640-2654; g) D. I. Ugwu, J. Conradie, *J. Mol. Struct.* **2023**, *1293*, 136275.

[3] a) A. B. Rolka, B. König, *Nat. Synth.* **2023**, *2*, 913-925; b) J.-H. Shen, M. Shi, Y. Wei, *Chem. Eur. J.* **2023**, *29*, e202301157.

[4] S. Roy, H. Paul, I. Chatterjee, *Eur. J. Org. Chem.* **2022**, e202200446.

[5] a) T. Rigotti, A. Casado-Sánchez, S. Cabrera, R. Pérez-Ruiz, M. Liras, V. A. de la Peña O'Shea, J. Alemán, *ACS Catal.* **2018**, *8*, 5928-5940; b) A. Gualandi, F. Calogero, A. Martinelli, A. Quintavalla, M. Marchini, P. Ceroni, M. Lombardo, P. G. Cozzi, *Dalton Trans.* **2020**, *49*, 14497-14505.

[6] a) R. Alonso, T. Bach, *Angew. Chem. Int. Ed.* **2014**, *53*, 4368-4371; b) J. R. Frost, S. M. Huber, S. Breitenlechner, C. Bannwarth, T. Bach, *Angew. Chem. Int. Ed.* **2015**, *54*, 691-695; c) A. Böhm, T. Bach, *Synlett* **2016**, *27*, 1056-1060; d) A. Tröster, R. Alonso, A. Bauer, T. Bach, *J. Am. Chem. Soc.* **2016**, *138*, 7808-7811; e) A. Hölzl-Hobmeier, A. Bauer, A. V. Silva, S. M. Huber, C. Bannwarth, T. Bach, *Nature* **2018**, *564*, 240-243; f) A. Tröster, A. Bauer, C. Jandl, T. Bach, *Angew. Chem. Int. Ed.* **2019**, *58*, 3538-3541; g) X. Li, C. Jandl, T. Bach, *Org. Lett.* **2020**, *22*, 3618-3622; h) M. Plaza, C. Jandl, T. Bach, *Angew. Chem. Int. Ed.* **2020**, *59*, 12785-12788; i) X. Li, R. J. Kutta, C. Jandl, A. Bauer, P. Nuernberger, T. Bach, *Angew. Chem. Int.*

Ed. **2020**, *59*, 21640-21647; j) M. Plaza, J. Großkopf, S. Breitenlechner, C. Bannwarth, T. Bach, *J. Am. Chem. Soc.* **2021**, *143*, 11209-11217; k) X. Li, J. Großkopf, C. Jandl, T. Bach, *Angew. Chem. Int. Ed.* **2021**, *60*, 2684-2688; l) T. Kratz, P. Steinbach, S. Breitenlechner, G. Storch, C. Bannwarth, T. Bach, *J. Am. Chem. Soc.* **2022**, *144*, 10133-10138.

[7] F. Mayr, L.-M. Mohr, E. Rodriguez, T. Bach, *Synthesis* **2017**, *49*, 5238-5250.

[8] a) F. Pecho, Y.-Q. Zou, J. Gramüller, T. Mori, S. M. Huber, A. Bauer, R. M. Gschwind, T. Bach, *Chem. Eur. J.* **2020**, *26*, 5190-5194; b) J. Lyu, A. Claraz, M. R. Vitale, C. Allain, G. Masson, *J. Org. Chem.* **2020**, *85*, 12843-12855; c) F. Pecho, Y. Sempere, J. Gramüller, F. M. Hörmann, R. M. Gschwind, T. Bach, *J. Am. Chem. Soc.* **2021**, *143*, 9350-9354; d) J. Lyu, M. Leone, A. Claraz, C. Allain, L. Neuville, G. Masson, *RSC Adv.* **2021**, *11*, 36663-36669; e) R. Takagi, T. Tanimoto, *Org. Biomol. Chem.* **2022**, *20*, 3940-3947; f) A. B. Rolka, N. Archipowa, R. J. Kutta, B. König, F. D. Toste, *J. Org. Chem.* **2023**, *88*, 6509-6522.

[9] a) X.-f. Tang, S.-h. Feng, Y.-k. Wang, F. Yang, Z.-h. Zheng, J.-n. Zhao, Y.-f. Wu, H. Yin, G.-z. Liu, Q.-w. Meng, *Tetrahedron* **2018**, *74*, 3624-3633; b) X.-F. Tang, J.-N. Zhao, Y.-F. Wu, Z.-H. Zheng, S.-H. Feng, Z.-Y. Yu, G.-Z. Liu, Q.-W. Meng, *Org. Biomol. Chem.* **2019**, *17*, 7938-7942; c) X.-F. Tang, J.-N. Zhao, Y.-F. Wu, S.-H. Feng, F. Yang, Z.-Y. Yu, Q.-W. Meng, *Adv. Synth. Catal.* **2019**, *361*, 5245-5252.

[10] a) W. Ding, L.-Q. Lu, Q.-Q. Zhou, Y. Wei, J.-R. Chen, W.-J. Xiao, *J. Am. Chem. Soc.* **2017**, *139*, 63-66; b) H. Yin, C.-J. Wang, Y.-G. Zhao, Z.-Y. He, M.-M. Chu, Y.-F. Wang, D.-Q. Xu, *Org. Biomol. Chem.* **2021**, *19*, 6588-6592.

[11] T. Gandini, L. Dolcini, L. Di Leo, M. Fornara, A. Bossi, M. Penconi, A. Dal Corso, C. Gennari, L. Pignataro, *ChemCatChem* **2022**, *14*, e202200990.

[12] J. A. Terrett, J. D. Cuthbertson, V. W. Shurtleff, D. W. C. MacMillan, *Nature* **2015**, *524*, 330-334.

[13] R. Sun, Y. Qin, S. Ruccolo, C. Schnedermann, C. Costentin, D. G. Nocera, *J. Am. Chem. Soc.* **2019**, *141*, 89-93.

[14] Generation of the Ni^{I} catalytic species from photoactive Ni^{II} complexes in the absence of a photocatalyst has also been reported. See: a) B. J. Shields, B. Kudisch, G. D. Scholes, A. G. Doyle, *J. Am. Chem. Soc.* **2018**, *140*, 3035-3039; b) S. I. Ting, S. Garakyaraghi, C. M. Taliaferro, B. J. Shields, G. D. Scholes, F. N. Castellano, A. G. Doyle, *J. Am. Chem. Soc.* **2020**, *142*, 5800-5810; c) L. Yang, H.-H. Lu, C.-H. Lai, G. Li, W. Zhang, R. Cao, F. Liu, C. Wang, J. Xiao, D. Xue, *Angew. Chem. Int. Ed.* **2020**, *59*, 12714-12719; d) D. A. Cagan, G. D. Stroscio, A. Q. Cusumano, R. G. Hadt, *J. Phys. Chem. A* **2020**, *124*, 9915-9922; e) D. A. Cagan, D. Bím, B. Silva, N. P. Kazmierczak, B. J. McNicholas, R. G. Hadt, *J. Am. Chem. Soc.* **2022**, *144*, 6516-6531; f) C. Cavedon, S. Gisbertz, S. Reischauer, S. Vogl, E. Sperlich, J. H. Burke, R. F. Wallick, S. Schrottke, W.-H. Hsu, L. Anghileri, Y. Pfeifer, N. Richter, C. Teutloff, H. Müller-Werkmeister, D. Cambié, P. H. Seeberger, J. Vura-Weis, R. M. van der Veen, A. Thomas, B. Pieber, *Angew. Chem. Int. Ed.* **2022**, *61*, e202211433.

[15] L. Dolcini, T. Gandini, R. Castiglioni, A. Bossi, M. Penconi, A. Dal Corso, C. Gennari, L. Pignataro, *J. Org. Chem.* **2023**, *88*, 14283-14291.

[16] a) J. Luo, J. Zhang, *ACS Catal.* **2016**, *6*, 873-877; b) E. Speckmeier, T. G. Fischer, K. Zeitler, *J. Am. Chem. Soc.* **2018**, *140*, 15353-15365.

[17] For examples of use of DA cyanoarenes in bifunctional catalysis, see: a) Ref. 8f; b) D. Chao, M. Zhao, *Dalton Trans.* **2019**, *48*, 5444-5449.

[18] L. Rasu, M. Amiri, S. H. Bergens, *ACS Appl. Mater. Interfaces* **2021**, *13*, 17745-17752.

[19] R. Ishimatsu, S. Matsunami, K. Shizu, C. Adachi, K. Nakano, T. Imato, *J. Phys. Chem. A* **2013**, *117*, 5607-5612.

[20] For an example of substituent effect on the PC's de-excitation pathway, see: H. Sayre, H. H. Ripberger, E. Odella, A. Zieleniewska, D. A. Heredia, G. Rumbles, G. D. Scholes, T. A. Moore, A. L. Moore, R. R. Knowles, *J. Am. Chem. Soc.* **2021**, *143*, 13034-13043.

[21] M. S. Oderinde, M. Frenette, D. W. Robbins, B. Aquila, J. W. Johannes, *J. Am. Chem. Soc.* **2016**, *138*, 1760-1763.

[22] a) A. M. Borys, *Organometallics* **2023**, *42*, 182-196; b) W. C. Still, M. Kahn, A. Mitra, *J. Org. Chem.* **1978**, *43*, 2923-2925; c) G. R. Fulmer, A. J. M. Miller, N. H. Sherden, H. E. Gottlieb, A. Nudelman, B. M. Stoltz, J. E. Bercaw, K. I. Goldberg, *Organometallics* **2010**, *29*, 2176-2179; d) Ref. 16a; e) Ref. 18; f) H. J. Davis, M. T. Mihai, R. J. Phipps, *J. Am. Chem. Soc.* **2016**, *138*, 12759-12762; g) R. Küng, A. Germann, M. Krüsmann, L. P. Niggemann, J. Meisner, M. Karg, R. Göstl, B. M. Schmidt, *Chem. Eur. J.* **2023**, *29*, e202300079; h) Y. M. Kim, S. Yu, *J. Am. Chem. Soc.* **2003**, *125*, 1696-1697; i) L. Yang, H. Li, H. Zhang, H. Lu, *Eur. J. Org. Chem.* **2016**, 5611-5615; j) G. Li, X. Zhao, K. Fang, J. Li, Y. She, *J. Org. Chem.* **2017**, *82*, 8634-8644; k) G. Gritzner, J. Kuta, *Pure Appl. Chem.* **1984**, *56*, 461-466; l) G. Gritzner, *Pure Appl. Chem.* **1990**, *62*, 1839-1858.